**Annales
Geophysicae**

Comparisons of refractive index gradient and stability profiles measured by balloons and the MU radar at a high vertical resolution in the lower stratosphere

H. Luce[1], G. Hassenpflug[2], M. Yamamoto[2], and S. Fukao[2]

[1]Laboratoire de Sondages Electromagnétiques de l'Environnement Terrestre, Université de Toulon et du Var, CNRS, La Garde, 83957, France
[2]Research Institute for Sustainable Humanosphere, Kyoto University, Uji, 611-0011, Japan

Abstract. Many experimental studies have demonstrated that VHF Stratosphere-Troposphere (ST) radar echo power is proportional to the generalized refractive index gradient squared M^2 when using a vertically oriented beam. Because humidity is generally negligible above the tropopause, VHF ST radars can thus provide information on the static stability (quantified by the squared Brunt-Väisälä frequency N^2) at stratospheric heights and this capability is useful for many scientific applications. Most studies have been performed until now at a vertical resolution of 150 m or more. In the present paper, results of comparisons between radar- and (balloon borne) radiosonde-derived M^2 and N^2 are shown at a better vertical resolution of 50 m with the MU radar (34.85° N, 136.15° E; Japan) by benefiting from the range resolution improvement provided by the multi-frequency range imaging technique, using the Capon processing method. Owing to favorable winds in the troposphere, the radiosondes did not drift horizontally more than about 30 km from the MU radar site by the time they reached an altitude of 20 km. The measurements were thus simultaneous and almost collocated. Very good agreements have been obtained between both high resolution profiles of M^2, as well as profiles of N^2. It is also shown that this agreement can still be improved by taking into account a frozen-in advection of the air parcels by a horizontally uniform wind. Therefore, it can be concluded that 1) the range imaging technique with the Capon method really provides substantial range resolution improvement, despite the relatively weak Signal-to-Noise Ratios (SNR) over the analyzed region of the lower stratosphere, 2) the proportionality of the radar echo power to M^2 at a vertical scale down to 50 m in the lower stratosphere is experimentally demonstrated, 3) the MU radar can provide stability profiles with a vertical resolution of 50 m at heights where humidity is negligible, 4) stable stratospheric layers as thin as 50 m or less have at least a horizontal extent of a few km to several tens of kilometers and can be considered as frozenly advected over scales of a few tens of minutes.

Keywords. Atmospheric composition and structure (Instruments and techniques) – Meteorology and atmospheric dynamics (Turbulence) – Radio science (Interferometry)

1 Introduction

The fact that VHF Stratosphere-Troposphere (ST) radars can provide in some circumstances a measure of the background static stability has been used many times for studying various atmospheric structures and phenomena such as the tropopause (e.g. Gage and Green, 1979; and recently Yamamoto et al., 2003), tropopause folds and meteorological fronts (e.g. Röttger, 1979; Larsen and Röttger, 1983; Fukao et al., 1989; Bertin et al., 2001). More generally speaking, the proportionality between the echo power P (corrected for the range (z) attenuation effects, i.e. $P.z^2$) and the square of the mean vertical gradient of the generalized potential refractive index M has been experimentally demonstrated from comparisons between radar and balloon observations (e.g. Tsuda et al., 1988; Hooper et al., 2004, and references therein). Most discrepancies at stratospheric heights have been explained by the effects of the horizontal inhomogeneity of the refractive index field, especially under conditions of mountain gravity wave activity, and by the (varying) horizontal separation between the instruments due to the balloon drift. At tropospheric heights, vertical variations of M^2 are dominated by humidity fluctuations which are usually much more intermittent and inhomogeneous, due to local convective processes and clouds, for example, and, consequently, the results of comparisons often show much larger discrepancies (e.g. Tsuda et al., 1988).

Correspondence to: H. Luce
(hubert.luce@lseet.univ-tln.fr)

In the present paper, we compare profiles of M^2 and the square of Brünt-Väisälä frequency N^2 in the stratosphere calculated at a vertical resolution of 50 m from MU radar echo power measurements and from measurements performed by 6 GPS Vaissala balloons launched at the radar site during an observational campaign of about 35 h on 8–10 May 2006. Such a high vertical resolution could be achieved with the MU radar, owing to the application of the range imaging mode used for improving the range resolution (Palmer et al., 1999; Luce et al., 2001). Chilson et al. (2001) showed similar but less detailed results of comparisons using data collected in range imaging mode at tropospheric heights with the SOUSY VHF radar.

The purpose of the present radar-balloon campaign was twofold. First, it was to validate the performances of the range imaging technique with the MU radar through comparisons with balloon measurements; and second, it was to study in more detail the small-scale structures of the lower atmosphere and in particular, the thin scattering layers of the lower stratosphere.

The theoretical background is first presented in Sect. 2. In Sect. 3, we present the balloon and radar experimental setups, and in Sect. 4 the methods and hypotheses used for estimating M^2 and N^2 at a vertical resolution of 50 m from balloon and radar measurements are explained. The results of comparisons are shown in Sect. 5 and conclusions are given in Sect. 6.

2　Theoretical background

Ottersten (1969) defined the vertical gradient of the generalized potential refractive index M as follows:

$$M = 77.6 \times 10^{-6} p/T \left\{ N^2/g + 15500q/T. \right.$$
$$\left. \left[N^2/g - (\partial \ln q/\partial z)/2 \right] \right\}, \tag{1}$$

where p, q, T are atmospheric pressure (hPa), specific humidity (g/g), and temperature (K), respectively. The parameter g is the acceleration of gravity (ms^{-2}). The squared Brunt-Väisälä frequency, which is a measure of the static stability, is given by:

$$N^2 = \frac{g}{T} \left(\frac{dT}{dz} + \Gamma \right). \tag{2}$$

The parameter $\Gamma \approx 10\,\mathrm{Kkm}^{-1}$ is the adiabatic lapse rate. Above the tropopause, humidity is generally negligible. Therefore, M is proportional to N^2 and to p/T, i.e. to the air density, which roughly decreases exponentially with height in the troposphere.

Two basic models of backscattering processes are often proposed for explaining the radar returns: partial (or Fresnel) reflection from laminar temperature and/or humidity sheets and scattering from isotropic turbulence. The former is quantified in terms of the partial reflection coefficient ρ and the

latter in terms of turbulent reflectivity η. Previous works have related these parameters to M^2. For the Fresnel reflection mechanism, VanZandt and Vincent (1983) showed that $P.z^2 \propto |\rho|^2 \propto M^2 E(2k)$, where $E(2k)$ is the spectrum of vertical displacements at the vertical scale of half of the radar wavelength. For the mechanism of scattering from isotropic turbulence, $P.z^2 \propto \eta \propto M^2 L_0^{4/3}$, where L_0 is the outer scale length of the turbulence spectrum (e.g. Gage and Balsley, 1980). The coefficients of proportionality between $P.z^2$ and $\{\eta, |\rho|^2\}$ are mainly related to radar parameters and wavelength (e.g. see Hooper et al., 2004, for more details). Thus, the two models do not provide a simple relation between the echo power P and M^2 because of the unknown quantities $E(2k)$ and L_0. However, all the experimental studies concluded that these factors do not play an important role and that they can be considered as constant (i.e. independent of z). Thus, in the present paper, we test the hypothesis that M^2 estimates from radar observations at a vertical resolution of 50 m are given by $M^2 = K P.z^2$, where K is a calibration constant estimated from the comparisons from balloon-derived M^2 estimates. As in Hooper et al. (2004), we will not try to distinguish the backscattering mechanisms in the present work. It is believed, however, that the partial reflection mechanism dominates, since radar echoes were aspect sensitive at the stratospheric heights during the experiment (not shown).

3　Balloon and radar experimental setup

During the observation campaign, 6 GPS balloons (hereafter noted B1, B2, etc.) were launched at the MU radar site. They provided pressure, relative humidity, temperature, zonal and meridional wind components at a time rate of 2 s. Table 1 shows the local time of their launch, as well as the tropopause altitude obtained from the temperature profiles. Figure 1 shows the balloon trajectories projected in the horizontal plane for the 6 flights. Small circles indicate the position of the balloons when crossing the height of the tropopause. Due to weak winds, the balloons did not drift more than about 30 km from the launch site by the time that they reached an altitude of 20 km. In particular, during the ascent of B3, the wind direction was northward and then westward in the troposphere and became south-eastward when approaching the stratosphere. The balloon drifted very close to the MU radar site just above the tropopause. Thus, the wind conditions were extremely favorable for comparisons between measurements from the two instruments even at stratospheric heights.

The MU radar was operated in a 5-frequency range imaging mode at ranges between 1.3 km and 20.3 km above the sea level (a.s.l.). The observations were carried out with a subpulse width of 1 μs (corresponding to an initial height resolution of 150 m) and an optimal pulse code of 16 moments. The radar parameters used were similar to those given by Luce et al. (2006). This observational mode was applied in 5 directions (vertical and 4 oblique beams aligned north,

Table 1. Launch time (LT) of the 6 GPS balloons and the tropopause height from temperature measurements.

	B1	B2	B3	B4	B5	B6
Time (LT)	8 May 20:54	9 May 00:00	9 May 02:56	9 May 08:55	9 May 20:54	10 May 00:02
Tropopause height (km)	12.96	12.76	12.76	12.78	14.15	14.67

east, south and west at a zenith angle of 10°) for estimating horizontal winds at a high vertical resolution (not shown). The collected data are processed with the adaptive filter-bank Capon method for estimating high-resolution Doppler spectra, as performed by Yu and Brown (2004) and Chilson (2004). The acquisition time for one record of 128 samples for the 5 directions is 40.96 s without a temporal gap between the records. The data processing is performed with an over-lapping factor of 2, so that profiles for the 5 directions are obtained every 20.48 s. A vertical sampling of 5 m has been applied but this value does not correspond to the vertical res-olution achieved by the Capon processing, since the vertical resolution depends on SNR. For comparisons with parame-ters estimated from balloon measurements, a vertical sam-pling of 50 m was applied. More detailed explanations are given in Sect. 4.2.

Figure 2 shows a time-height cross section of echo power after the Capon processing with a 5-m altitude sampling from 9 May, 09:30 LT until 10 May, 07:07 LT. The crosses indicate the position of the tropopause provided by B4, B5 and B6 (see Table 1). Below 4–5 km, the intense echoes present large time-height variations likely due to cloud activity, since the relative humidity profiles provided by the balloon measure-ments revealed values close to or equal to 100% (not shown). Above 8 km, and especially in the lower stratosphere, the stratification is much more pronounced with long-lasting thin echoing layers. A tropopause fold occurs around 10 May, 18:00 LT and a thick region of echo power minimum is ob-served around 12 km in the core of the jet stream, according to the wind measurements (not shown).

4 M^2 and N^2 estimation methods

4.1 Estimations from balloon measurements

The vertical sampling of the pressure P, temperature T and humidity U profiles typically ranges between 10 and 20 m, depending on the balloon ascent rate. The first step was to re-sample the PTU profiles at a constant step of 15 m after applying a spline cubic interpolation. Figure 3 shows the temperature fluctuation spectrum for stratospheric heights and for B1. It clearly reveals a slope of -3 down to 10^{-2}–2.10^{-2} cy m^{-1} (i.e. vertical scales of $\sim$50–100 m). This slope is understood as a signature of saturated gravity waves (e.g. Fritts et al., 1988; Sidi and Dalaudier, 1989). At
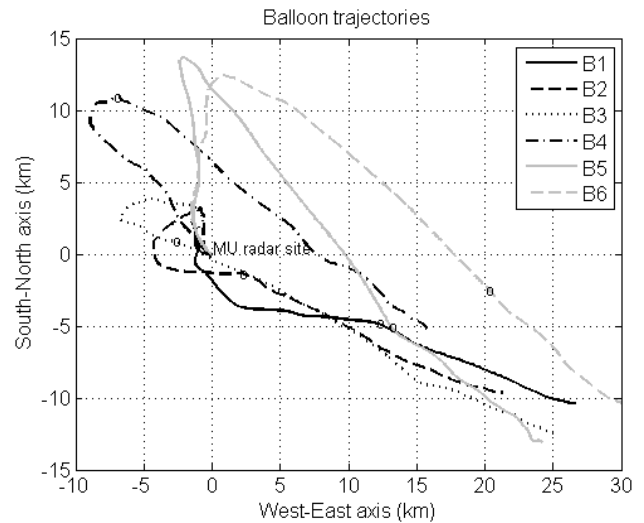

Fig. 1. Trajectories of the six GPS Vaissala radiosondes launched at the MU radar site during the experiment. Small circles indicate the position of the balloons when crossing the tropopause.

smaller scales, the slope is close to 0, i.e. the fluctuations are dominated by the instrumental noise. Therefore, estimations of parameters at a vertical scale of 15 m would be strongly affected by the noise. The PTU profiles have been filtered by using a low-pass filter with a cutoff wavelength of 100 m,, so that a vertical resolution of 50 m was obtained. The N^2 pro-files from balloon measurements (hereafter noted N_b^2) at this vertical resolution are estimated from the low-pass filtered temperature profiles by using Eq. (2). The M^2 profiles (here-after noted M_b^2) with and without humidity are then obtained by using Eq. (1).

4.2 Estimations from radar echo power measurements

With the radar parameters used, SNR maxima at the ini-tial range resolution (150 m) were typically between 0 and 20 dB in the lower stratosphere. According to simulations performed by Palmer et al. (1999) and Luce et al. (2001), the resolution performances of the Capon method should be significantly reduced. Thus, in accordance with the verti-cal resolution of 50 m of the M_b^2 and N_b^2 profiles, the high resolution profiles of power P_c given by the Capon process-ing, and corrected for the range-squared effects (i.e. $P_c.z^2$) have been re-sampled at a step of 50 m at the altitudes of
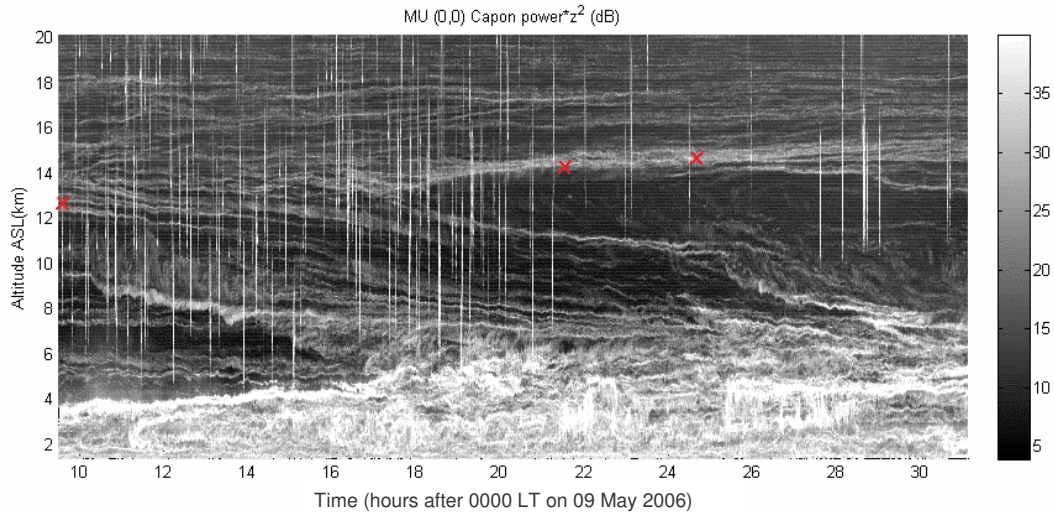
Fig. 2. Example of time-height plots of power after Capon processing, compensated by the range attenuation effects at a time sampling of 20.48 s and a vertical sampling of 5 m from 1.225 km to 19.975 km and from 9 May 2006 at 09:30 LT until 10 May 2006 at 07:07 LT. The red crosses indicate the tropopause height inferred from B4, B5 and B6. Vertical bright lines correspond to airplane echoes and should not be considered.
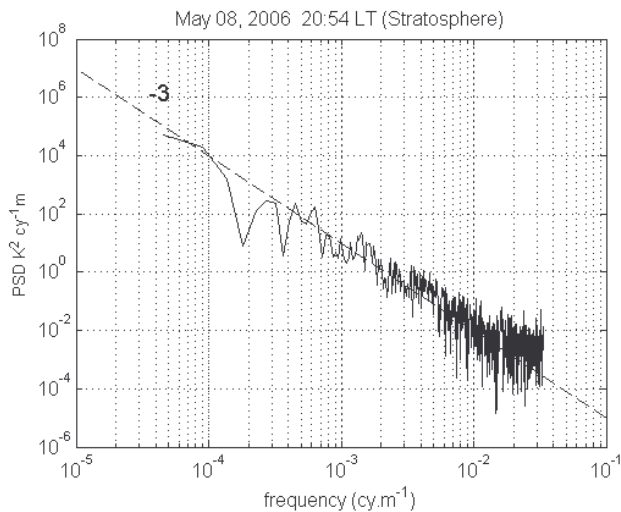

Fig. 3. Temperature fluctuation spectrum obtained in the lower stratosphere estimated from the temperature measurements with B1.

the points of the M_b^2 (N_b^2) profiles. This vertical sampling should be more consistent with the effective resolution improvement provided by the Capon processing in this altitude range. It still represents a factor 3 with respect to the initial range resolution. The method used for estimating the Capon power P_c has been described by Yu and Brown (2004) and Chilson et al. (2004).

The profiles of radar-derived M^2 (hereafter noted M_r^2) described in Sect. 5.1 result from a time averaging of 71 individual profiles of $P_c.z^2$ (i.e. over about 25 min) during the ascent of the radiosondes between altitudes of 10.5 and 20 km.

The six M_r^2 profiles have been calculated with the constant $K_{dB}=-231$ dB, so that $<M_r^2>$ is equal to $<M_b^2>$, where the average $<>$ is performed on all the available values. Assuming a dry air and from (A1), we have:

$$N^2 = \frac{g}{77.6\ 10^{-6}} \frac{T}{p} |M| , \qquad (3)$$

where the $|.|$ operator indicates that we use the restrictive hypothesis that N^2 is positive or null everywhere, i.e. that the stratosphere is everywhere stable or neutral at a vertical scale of 50 m. According to the N_b^2 profiles shown later in Sect. 5, this hypothesis was fulfilled in the present data set. However, local (slightly) superadiabatic gradients (i.e. negative potential temperature gradients) can occur due to overturning produced by Kelvin-Helmholtz and convective instabilities. Such gradients were observed at vertical scales of a few tens of meters by Mantis and Pepin (1971) in the stratosphere. Very few have been found in very high vertical resolution temperature profiles described by Dalaudier et al. (1994) and even at a vertical scale of 12.8 m in the temperature profiles collected near the MU radar (Figs. 5–7 of Gavrilov et al., 2005). Consequently, it is expected that errors should only occur occasionally and locally.

Equation (3) shows that T/p must be estimated. Hooper et al. (2004) used the fact that this is proportional to $1/\rho$, where ρ is the air density, assuming air as a perfect gas. They used the standard exponential model $\rho=\rho_0 \exp(-z/H)$, where ρ_0 is the density at the sea level, $H=RT/g$ is a mean scale height of the atmosphere (of the order of 8 km) and R is the specific constant of air. However, this model is well adapted for tropospheric heights, and substantial discrepancies can occur at stratospheric heights. In the current work,
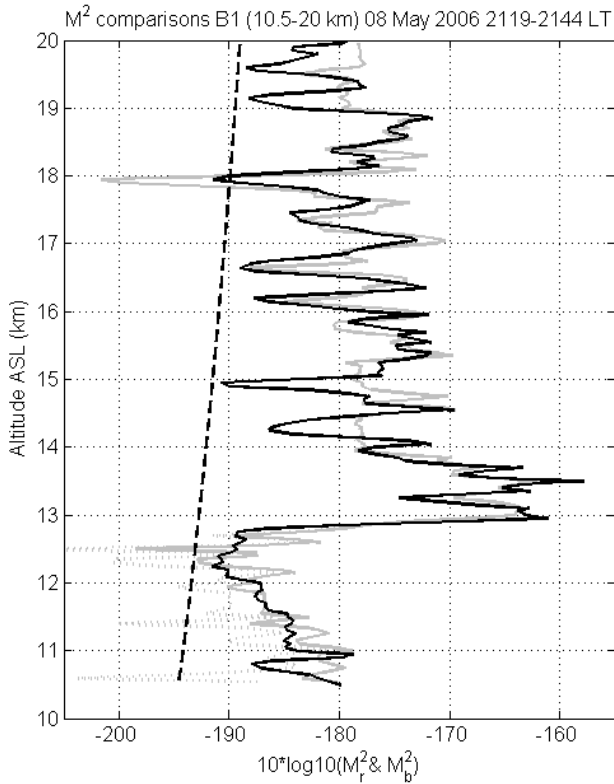
Fig. 4a. Comparisons for the flight B1 between profiles at a vertical resolution of 50 m of M_r^2 (black line) and M_b^2 (grey solid line for the profiles including humidity and grey dotted line without humidity). An approximate radar noise level is shown as a black dashed line.
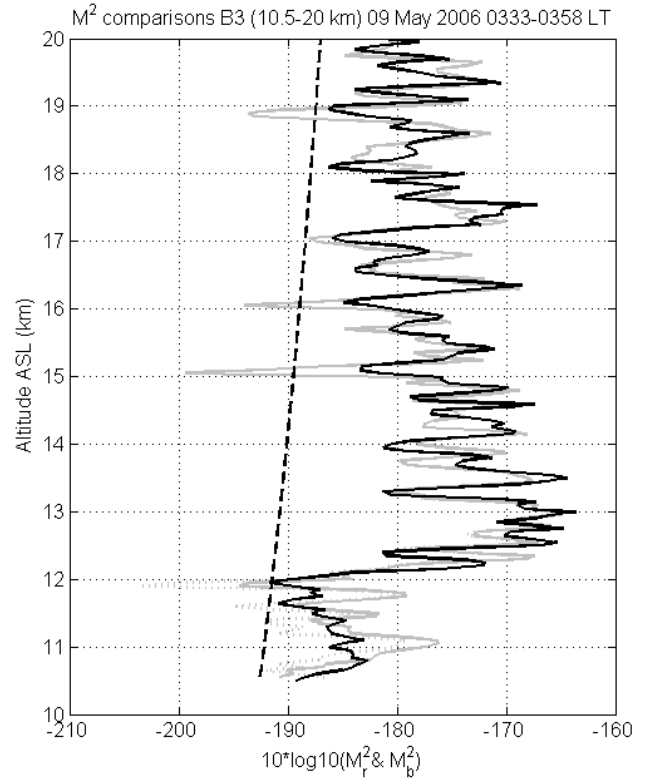
Fig. 4b. Same as Fig. 4a but for B3.

since pressure and temperature are available from radiosondes, they could be used for estimating T/p. This method would not be of great interest because the objective is to retrieve the parameters without using data from PTU GPS radiosondes. It can be noted from Eq. (3) that an accurate value of T is not crucial since T does not usually vary by more than 10% between 10 and 20 km. Pressure can play a more important role especially at high altitudes, where pressure values given by the model can strongly differ from the measured values. An alternative method is to use the temperature and pressure profiles from the closest meteorological radiosondes in time and distance. We used the averaged temperature and pressure profiles measured from the meteorological stations of Yonago (35.4° N, 133.3° E) and Hamamatsu (34.8° N, 137.7° E), since they are, in principle, always available. The MU radar (34.85° N, 136.15° E) is approximately aligned with the position of these 2 stations. The balloons B1, B4 and B5 were launched at the same time as meteorological radiosondes while the time difference was +3 h for B2, −6 h for B3, and +3 h for B6. The averaged pressure profiles did not differ by more than 1% only with respect to the pressure profiles measured by the GPS radiosondes between 10 and 20 km. They are thus well adapted for our objective.

The averaged pressure and temperature profiles noted as $\bar{p}_m$ and $\bar{T}_m$, respectively, have been re-sampled at a step of 50 m at the altitudes of M^2 profiles. Consequently, the squared BV frequency is estimated from radar measurements by:

$$N_r^2 = \frac{g}{77.6\ 10^{-6}} \frac{\overline{T_m}}{\overline{p_m}} \sqrt{K P_c z^2}.$$ (4)

5 Results of comparisons

5.1 M^2 profiles

Figures 4a, b, c show comparisons between M_b^2 and M_r^2 profiles between 10.5 km and 20 km a.s.l. at a vertical resolution of 50 m for three selected flights, B1, B3 and B5, respectively. Except below the tropopause for B1, the echoes were significantly aspect sensitive (about 10–20 dB, not shown), indicating the absence of intense turbulent layers producing isotropic echoes above the tropopause.

The profiles of M_b^2 with humidity and without humidity are given in solid and dotted grey lines, respectively. As expected, the contribution of the humidity in M_b^2 is negligible in the altitude range considered in the present work, except below the tropopause mainly for B1 (Fig. 4a). It is observed that the M_b^2 profiles and the M_r^2 profiles agree very well in the stratosphere, despite the 25-min time averaging of the radar
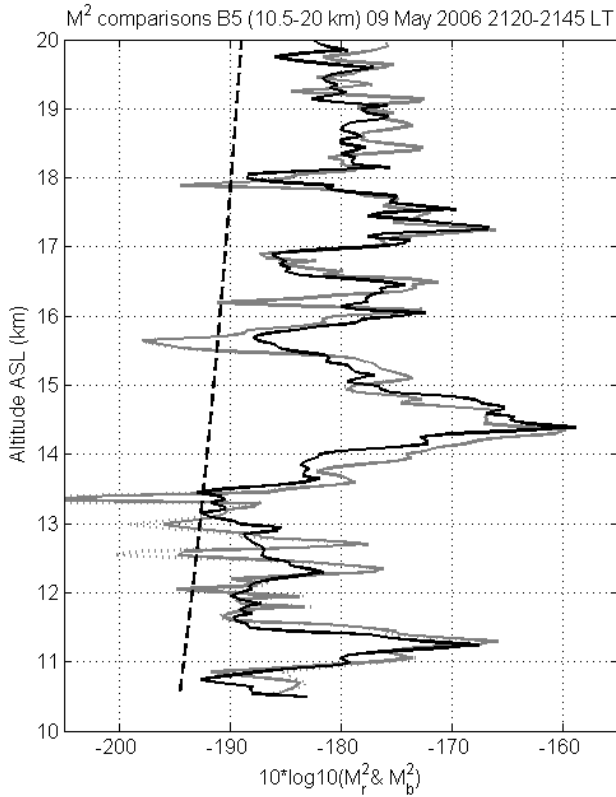
Fig. 4c. Same as Fig. 4a but for B5.

Fig. 5. Comparison of M_r^2 and M_b^2 for the 6 balloon flights and between 10.5 and 20 km.

profiles. In particular, the positions of the main extrema in the radar-deduced profiles correspond well with those found in the balloon-deduced profiles. This result indicates that the observed thin stratospheric layers did not evolve significantly during a time scale of 25 min. The very deep minima in the M_b^2 profiles are not always well reproduced in the M_r^2 profiles (for instance, below 18 km in Fig. 4a, above 15 km and 16 km and below 19 km in Fig. 4b), because the radar profiles reached their detection threshold and they resulted from a time-averaging. Below the tropopause, the agreement is quite poor and only the main tendencies are reproduced; the M_b^2 profiles reveal a higher variability with height with local (weak) peaks (for example, Fig. 4b below 12 km). This result is compatible with the more intermittent and inhomogeneous characteristics of the weakly stable upper troposphere (e.g. Worthington, 2004). Thus, the averaging procedure affects more significantly the quality of the comparisons of the profiles at tropospheric heights.

It is interesting to note that the profiles for B1 and B3 (launched before the tropopause fold) present different features from the profiles for B5 (launched after the tropopause fold). The latter show thicker peaks separated by deep minima at 15.5 km, 16.8 km and 18 km. It is not clear if this difference can be attributed to the folding event and/or to the presence of the jet stream or not. This topic should be the subject of a future work.
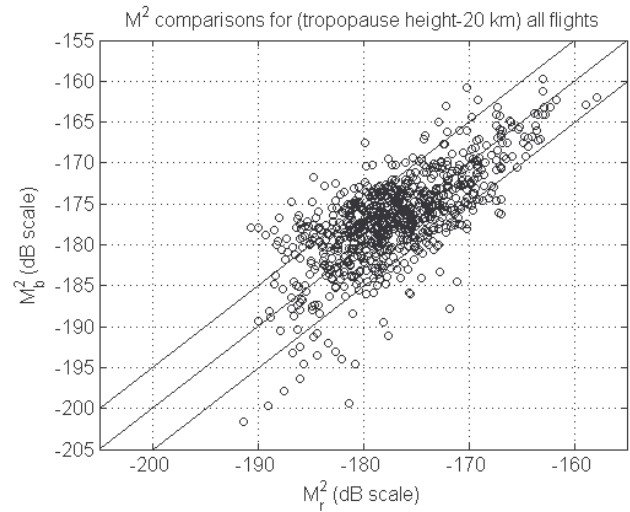
Both M_b^2 and M_r^2 profiles reveal thin peaks (smoothed at the initial resolution of 150 m, not shown), for example, between 12 and 15 km in Fig. 4b. This may indicate scattering layers even thinner than 50–100 m. The good correspondence between the profiles also indicates that their horizontal extent can exceed a few km. The inspection of the power maps, as in Fig. 2, show that they can persist for several hours. Figure 5 shows a comparison analysis between M_r^2 and M_b^2 using the 6 profiles. Most points are found between $+/-5$ dB from the diagonal. Table 2 shows cross-correlation coefficients and standard deviation of the difference $M_r^2 - M_b^2$ for 10.5–20 km and for each flight. The cross-correlation coefficients range within 0.51 (B4) and 0.84 (B1) and the standard deviations between 3.68 dB and 6.82 dB. It is important to indicate that the analysis of B4 may be affected by airplane echoes which strongly affected the radar measurements during this flight (5 events instead of 1 or 0 for the other selected observation periods). The corrupted data have been systematically rejected after visual inspection of the power profiles but residual spurious values, difficult to separate from atmospheric echoes, may still be present. Thus, the relatively low correlation for B4 may not be representative.

The agreement is sometimes slightly better than the one obtained by Tsuda et al. (1988), who used a vertical resolution of 150 m. The better agreement here is likely due to a smaller horizontal distance between the radar and the balloons, even if this effect was not discussed by Tsuda et al. (1988). The conditions of comparisons were thus suitable for confirming the good performances of the range imaging technique with the Capon processing.
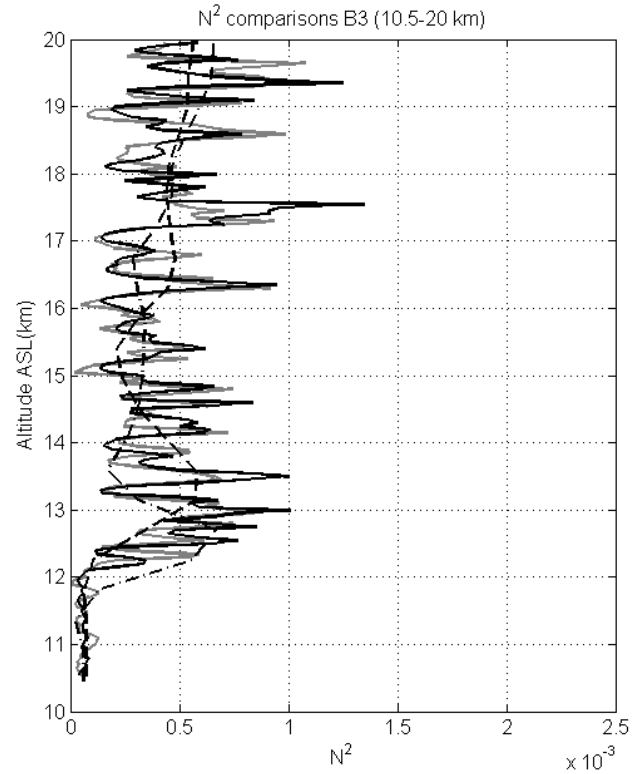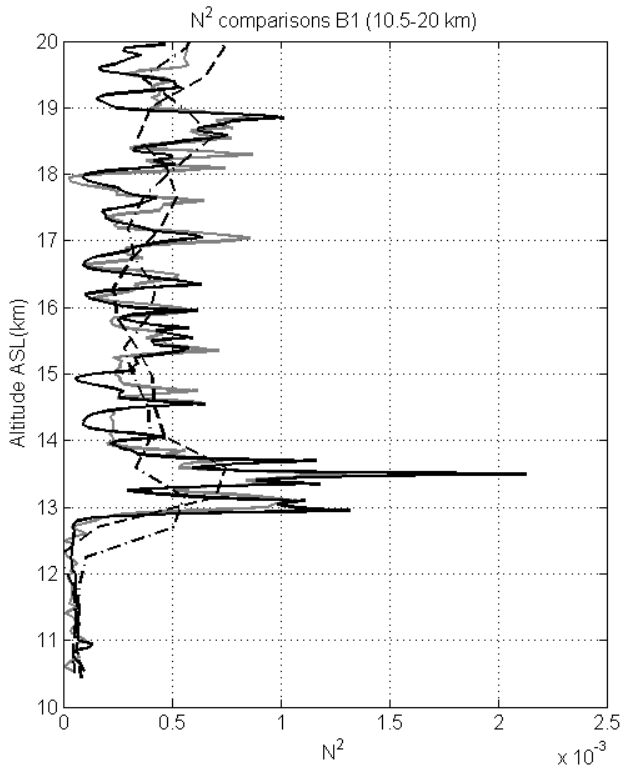
Fig. 6a. Comparisons between profiles of N^2 estimated from balloon data (grey line) and from radar echo power (black line) with a vertical resolution of 50 m. The dashed and dot-dashed lines show N^2 profiles estimated from the meteorological balloon data at Hamamatsu (34.8° N, 137.7° E) and Yonago (35.4° N, 133.3° E), respectively, at a vertical sampling of 450 m. The radar profile used the averaged pressure and temperature profiles measured by the closest (in time) meteorological radiosondes at Yonago and Hamamatsu around the MU radar site.

Fig. 6b. Same as Fig. 6a but for B3.

Table 2. Cross-correlation coefficients and standard deviation of the difference $M_r^2 - M_b^2$ for 10.5–20 km.

	B1	B2	B3	B4	B5	B6
Corr. Coef	0.84	0.83	0.77	0.51	0.80	0.69
σ (dB)	3.96	3.68	4.35	6.82	4.72	5.30

5.2 N^2 profiles

Figures 6a, b, c show comparisons between the profiles of N_r^2 and N_b^2 (in linear scale as it is often used to be in the literature) for B1, B3 and B5 and comparisons for the 6 balloon flights together are shown in Fig. 7. The agreements are quantitatively very good, indicating that the proposed method used for retrieving the static stability at a high vertical resolution from the MU radar in range imaging mode works well. The agreement is even good below the

tropopause because the linear scale "annihilates" the errors for small values. A threshold effect can be seen in Fig. 7 for small N_r^2 values and results from the radar noise level. The minimum N_r^2 detectable is about 4.10^{-5} rad² s⁻² and is mainly reached in the upper troposphere. As already mentioned earlier, it has to be noted that the N_b^2 profiles do not reveal negative values (as well as in the 3 other profiles, not shown). Both profiles present strong peaks that can exceed 10^{-3} rad² s⁻². They are likely produced by intense local temperature gradient sheets, similar to those observed very often in groups in high vertical resolution (20 cm) temperature measurements by balloons (Dalaudier et al., 1994) and in temperature profiles obtained in similar conditions near the MU radar (not published). The good agreement thus suggests that the MU radar in range imaging mode can resolve and monitor the thin regions where temperature sheets are embedded. For information, the N^2 profiles at a coarse vertical resolution obtained from the meteorological balloon data at Yonago and Hamamatsu meteorological stations are also shown.

5.3 Effects of the advection by the horizontal wind

A good agreement between the radar- and balloon-derived profiles has been found but a more thorough examination of Figs. 4 and 6 reveals significant discrepancies especially for B1 between 14 km and 15.3 km altitudes. The radar-derived
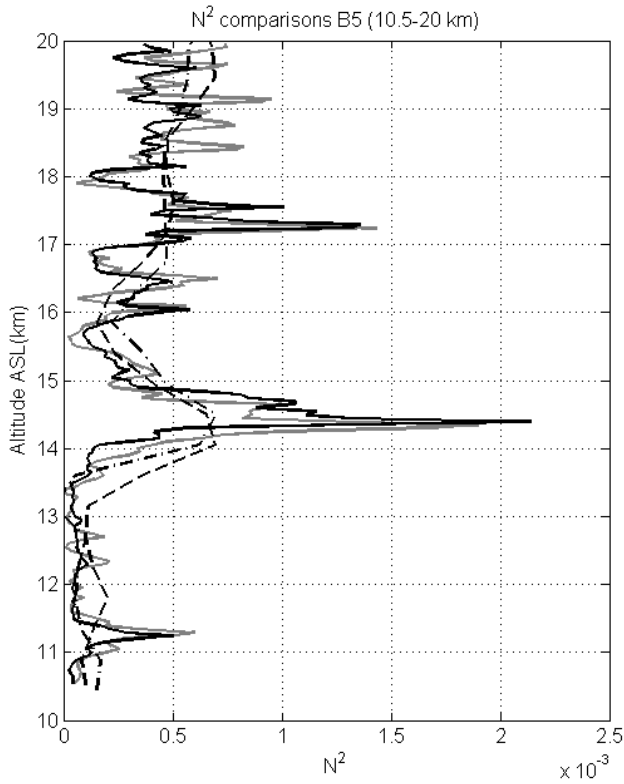
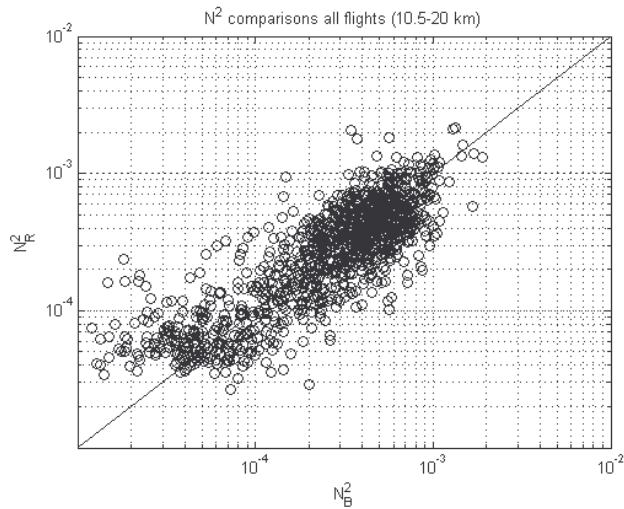**Fig. 6c.** Same as Fig. 6a but for B5.

Fig. 7. Comparisons of N_r^2 and N_b^2 for the 6 balloon flights and between 10.5 and 20 km.

profiles show a single thin peak at 14.5 km while 2 peaks of similar intensity are observed in the balloon-derived profiles at 14.5 km and 14.7 km. In addition, a maximum of N_r^2 and M_r^2 is found just above 14 km but does not appear in the N_b^2 (M_b^2) profiles. For the second case, the discrepancy could have an instrumental origin, as a careful inspection of
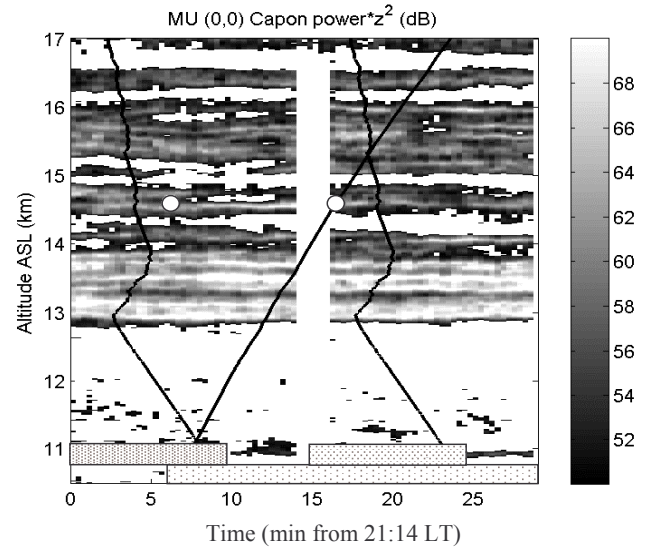

Fig. 8. Close-up of the height-time intensity plot of echo power (compensated from the range attenuation effects) after the Capon processing for about 30 min after the beginning of the experiment. The oblique line indicates the balloon path. The temperature profile (black) adjusted to the plot is plotted twice for comparing with the power map at two different times. The light, moderate and heavy grey rectangles represent the time period used for averaging the power profiles shown in Fig. 4a (6a), Figs. 10a and b, respectively. The white circle on the balloon path line is the position analyzed in Fig. 9 and the second white circle plotted 10 min before would correspond to the conditions met by the balloon if the frozen-in advection was taken into account.

the original temperature profile between 14 km and 14.5 km revealed a remarkable linear decrease with height, indicating that data were probably missing and replaced by a linear interpolation. Therefore, the results in this altitude range should be considered with caution. In the following, we only focus our attention on the maxima at 14.5 km and 14.7 km.

Figure 8 shows a time-height intensity plot of vertical echo power after the Capon processing between 10.5 km and 17 km for about 30 min after the beginning of the experiment. The balloon path is indicated, as well as the temperature profile. In accordance with the N_b^2 profiles, the temperature profile reveals two successive stable gradients of about 50 m in thickness around 14.5 km and 14.7 km. The power map indicates a strong, long-lasting echoing layer at 14.5 km but a much weaker one at 14.7 km at the position indicated by a white circle along the line, indicating the balloon altitude versus time. About 10 min earlier, at the position of the second white circle, the echoing layer at 14.7 km was associated with a peak of power similar to the echoing layer at 14.5 km, indicating that the conditions seen by the radar at that time were more compatible with those met by the balloon. This can occur if inhomogeneous parcels of air are advected by the horizontal wind. In order to check this hypothesis, we have considered the trajectory of the air parcels for B1 (Figs. 9

and 10). At an altitude of 14.5 km, the wind speed was $u=31.2\,\mathrm{ms^{-1}}$, according to the GPS balloon measurements, and its direction was 107 degrees from the north. The horizontal distance d between the balloon and the MU radar was 19.17 km. Assuming a uniform and constant horizontal wind in the horizontal plane, simple geometric calculations show that the air parcels met by the balloon at this altitude passed at the nearest horizontal distance southeastward from the radar at $d=19.04$ km from the balloon position. This minimal distance d_{min} is 1.6 km (see Fig. 9), i.e. only twice the horizontal width of the radar beam at this altitude. Since the balloon was at the altitude of 14.5 km at about 21:30 LT, the same air parcels were most likely observed by the MU radar about $\Delta t = d/u \approx 10$ min before, i.e. at the time indicated by the white circle in Fig. 8 (about 21:20 LT). The same parameters, i.e. the wind speed u, the distance d, the minimal distance d_{min} and the time lag Δt are shown in Fig. 10 for all the altitudes between 10.5 km and 20 km. It can be noted that the profile of d_{min} presents large values and large fluctuations above 16 km due to strong changes in wind direction likely related to gravity waves (not shown). Also, $|\Delta t|$ significantly increases due to the increasing distance d and the decreasing wind speed u. For instance, at 19 km, the air parcel met by the balloon may have passed nearby the radar at 8 km distance about 1 h before. Thus, large discrepancies between the comparisons might occur at the highest altitudes because of large values of d, d_{min} and $|\Delta t|$. M_r^2 profiles averaged over about 10 min from 21:14 LT until 21:24 LT are shown in Fig. 11b and the results obtained after a 10-min averaging between 21:29 LT and 21:39 LT during the balloon flight are shown in Fig. 11a. The latter shows features very similar to the profile in Fig. 4a, obtained after a longer time averaging of 25 min. The agreement between the profiles is significantly better after taking the frozen-in advection into account, not only between 14.5 km and 14.7 km but also at higher altitudes between 15 km and 16.5 km, indicating that the advection effects are also important in this altitude range. In terms of correlation, there is a slight improvement, since the correlation coefficient between the M_r^2 profiles and the M_b^2 profiles (shown in Fig. 11b) is 0.851 instead of 0.79 (Fig. 11a) and 0.84 (Fig. 4a). The same procedure has been applied for the other flights but no significant improvement has been obtained because there was no disagreement, such as the one shown in Fig. 11, except for B3, where the peaks are better reproduced below 12.4 km and between 13.5 km and 14.5 km (not shown).

Consequently, the present analysis revealed that the local discrepancies between the radar- and balloon-derived profiles when using the method described in Sects. 5.1 and 5.2 can mostly be explained by the horizontal inhomogeneity of thin stable layers (frozenly) advected by the wind, and not by the use of an inappropriate model. In other words, the contribution of the unknown quantities $E(2k)$ and L_0 in the models used (see Sect. 2) is negligible, even at a vertical scale of 50 m.
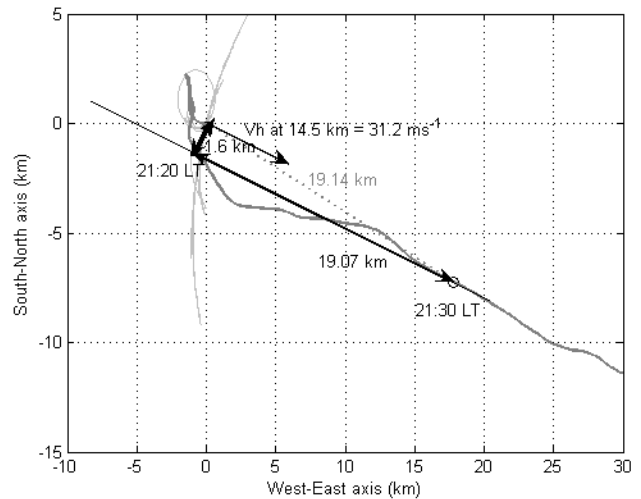

Fig. 9. (Heavy grey): Balloon B1 trajectory in the horizontal plane. (Light grey) the closest positions of the air parcels from the radar site, assuming a frozen-in advection in an uniform and constant horizontal wind. The particular case of an altitude of 14.5 km is also shown (see text for more details).

6 Conclusions

In the present work, we have described comparisons of radar- and balloon-derived M^2 and N^2 profiles between 10.5 km and 20 km, i.e. approximately in the lower stratosphere, with a vertical resolution of 50 m. Such a high vertical resolution could be achieved with the MU radar, owing to the multi-frequency range imaging technique with the Capon processing method. From these comparisons, it can be concluded that:

1. the range imaging technique really provides substantial range resolution improvement in the lower stratosphere, despite low SNR (typically between 0–20 dB),

2. the proportionality of the radar echo power to M^2 at a vertical scale as small as 50 m in the lower stratosphere is demonstrated. The discrepancies can be explained by the horizontal inhomogeneity of the thin stable layers which can be assumed to be frozen and advected over a few tens of minutes. The effect of other parameters, such as the spectrum of vertical displacements and the outer scale of turbulence, can be ignored, at least at a first approximation,

3. the MU radar in range imaging mode can provide N^2 profiles with a vertical resolution of 50 m in the lower stratosphere. We propose a method based on the use of rough measurements of temperature and pressure from the surrounding meteorological stations,
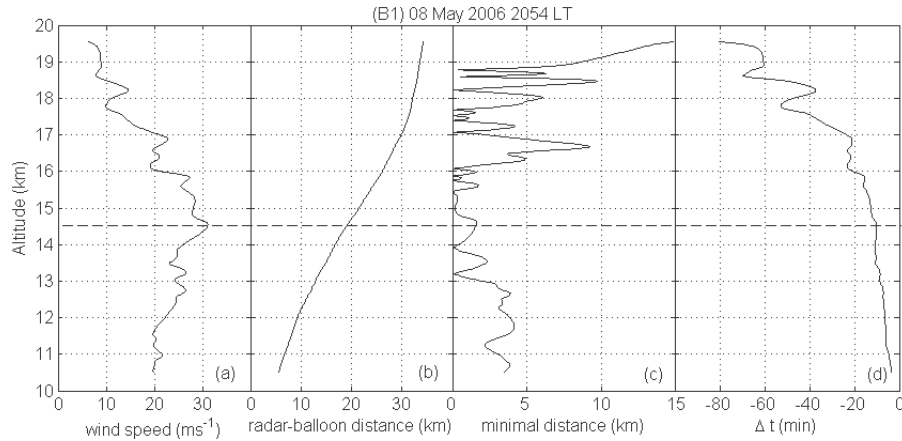
Fig. 10. (a) Wind speed (ms^{-1}) measured by B1 between 10.5 and 20 km. (b) The corresponding horizontal distance (km) between the radar and the balloon. (c) Minimal distances between the radar and the air parcels met by the balloon, assuming a frozen-in advection of the parcels in a constant and homogeneous wind in the horizontal plane. (d) The corresponding time delay between the passage to the closest location from the radar and the location of the balloon.
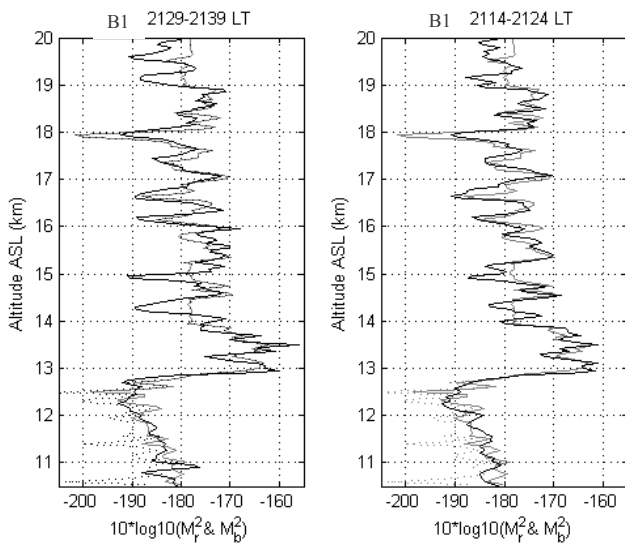

Fig. 11. (Left) Same as Fig. 4a after a 10-min averaging between 21:29 and 21:39 LT during the balloon flight. (Right) Same as left after a 10-min averaging between 21:14–21:24 LT in order to take into account the advection of the air parcels by the wind.

4. some stable stratospheric layers as thin as 50 m or less have at least a horizontal extent of a few km to several tens of kilometers.

References

Bertin, F., Campistron, B., Caccia, J. L., and Wilson, R.: Mixing processes in a tropopause folding observed by a network of ST radar and lidar, Ann. Geophys., 19, 953–963, 2001, http://www.ann-geophys.net/19/953/2001/.

Chilson, P. B., Palmer, R. D., Muschinski, A., Hooper, D. A., Schmidt, G., and Steinhagen, H.: SOMARE-99: A demonstrational field campaign for ultrahigh-resolution VHF atmospheric profing using frequency diversity, Radio Sci., 36, 695–707, 2001.

Chilson, P. B.: The retrieval and validation of Doppler velocity estimates from range imaging, J. Atmos. Ocean. Technol., 21, 1033–1043, 2004.

Dalaudier, F., Sidi, C., Crochet, M., and Vernin, J.: Direct evidence of sheets in the atmospheric temperature field, J. Atmos. Sci., 51, 237–248, 1994.

Fritts, D. C., Tsuda, T., Sato, T., Fukao, S., and Kato, S.: Observational evidence of a saturated gravity wave spectrum in the troposphere and lower stratosphere, J. Atmos. Sci., 45, 1741–1759, 1988.

Fukao, S., Yamanaka, M. D., Matsumoto, H., Sato, T., Tsuda, T., and Kato, S.: Wind fluctuations near a Cold vortex-tropopause funnel system observed by the MU radar, Pure Appl. Geophys., 130, 463–480, 1989.

Gage, K. S. and Balsley, B. B.: On the scattering and reflection mechanisms contributing to clear air echoes from the troposphere, stratosphere and mesosphere, Radio Sci., 15, 243–257, 1980.

Gage, K. S. and Green, J. L.: Tropopause detection by partial specular reflection using VHF radar, Science, 203, 1238–1240, 1979.

Gavrilov, N. M., Luce, H., Crochet, M., Dalaudier, F., and Fukao, S.: Turbulence parameter estimations from high-resolution balloon temperature measurements of the MUTSI-2000 campaign, Ann. Geophys., 23, 2401–2413, 2005, http://www.ann-geophys.net/23/2401/2005/.

Hooper, D. A., Arvelius, J., and Stebel, K.: Retrieval of atmospheric stability from MST radar return signal power, Ann. Geophys., 22,

3781–3788, 2004,
http://www.ann-geophys.net/22/3781/2004/.

Larsen, M. F. and Röttger, J.: Comparison of tropopause height and frontal boundary locations based on radar and radiosonde data, Geophys. Res. Lett., 10, 325–328, 1983.

Luce, H., Yamamoto, M., Fukao, S., Hélal, D., and Crochet, M.: A Frequency radar Interferometric Imaging applied with High Resolution Methods, J. Atmos. Sol. Terr. Phys., 63, 221–234, 2001.

Luce, H., Hassenpflug, G., Yamamoto, M., and Fukao, S.: High-resolution vertical imaging of the troposphere and lower stratosphere using the new MU radar system, Ann. Geophys., 24, 791–805, 2006,
http://www.ann-geophys.net/24/791/2006/.

Mantis, H. T. and Pepin, T. J.: Vertical temperature structure of the free atmosphere at mesoscale, J. Geophys. Res., 76, 8621–8628, 1971.

Ottersten, H.: Mean vertical gradient of potential refractive index in turbulent mixing and radar detection of CAT, Radio Sci., 4, 1247–1249, 1969.

Palmer, R. D., Yu, T.-Y., and Chilson, P. B.: Range imaging using frequency diversity, Radio Sci., 34(6), 1485–1496, doi:10.1029/1999RS900089, 1999.

Röttger, J.: VHF radar observations of a frontal passage, J. Appl. Meteorol., 18, 85–91, 1979.

Sidi, C. and Dalaudier, F.: Temperature and heat flux spectra in the turbulent buoyancy subrange, Pure Appl. Geophys., 130, 547–569, 1989.

Tsuda, T., May, P. T., Sato, T., Kato, S., and Fukao, S.: Simultaneous observations of reflection echoes and refractive index gradient in the troposphere and lower stratosphere, Radio Sci., 23, 655–665, 1988.

Van Zandt, T. E. and Vincent, R. A.: Is VHF Fresnel reflectivity due to low frequency buoyancy waves?, Handbook for MAP, Vol. 9, 78–80, Middle Atmosphere Program, University of Illinois, Urbana, 1983.

Worthington, R.: All-weather volume imaging of the boundary layer and tropopshere using the MU radar, Ann. Geophys., 22, 1407–1419, 2004,
http://www.ann-geophys.net/22/1407/2004/.

Yamamoto, M. K., Fujiwara, M., Horinouchi, T., Hashiguchi, H., and Fukao, S.: Kelvin-Helmholtz instability around the tropical tropopause observed with the Equatorial Atmosphere Radar, Geophys. Res. Lett., 30(9), 1476, doi:10.1029/2002GL016685, 2003.

Yu, T.-Y. and Brown, W. O. J.: High-resolution atmospheric profiling using combined spaced antenna and range imaging techniques, Radio Sci., 39, RS1011, doi:10.1029/2003RS002907, 2004.